[Review] www.whxb.pku.edu.cn

宽带隙 *p* 区金属氧化物/氢氧化物对苯的光催化降解

李朝晖 刘 平 付贤智*
(福州大学光催化研究所, 省部共建国家重点实验室培育基地, 福州 350002)

摘要: 苯具有高毒性和致病性, 是空气中最为常见的挥发性有机污染物. 以 TiO_2 为代表的半导体光催化氧化技术是一种理想的环境治理技术, 已广泛应用于一般室内挥发性有机物(VOCs)的去除. 然而在处理苯等难降解有机污染物时, 由于在催化剂表面生成难被降解的聚合物中间产物, 往往导致 TiO_2 光催化剂的失活. 开发可在常温下使用的降解苯系污染物的高效光催化剂对于推广光催化技术在苯污染治理中的应用具有重大的意义. 最近我们研究所开发出一系列宽带隙 *p* 区金属氧化物/氢氧化物光催化剂, 它们对苯系污染物的光催化降解显示出很好的活性和稳定性, 是一类极有前景的降解苯系污染物的新型光催化剂. 在这篇文章中, 我们总结这类宽带隙 *p* 区金属氧化物/氢氧化物光催化剂的制备及其光催化降解苯的活性, 对其不同于 TiO_2 的光催化机理, 及其结构和光催化性能之间的关系进行初步的探讨.

关键词: 光催化; 苯; 降解; p-区金属氧化物/氢氧化物
中图分类号: O6

Wide Bandgap *p*-Block Metal Oxides/Hydroxides for Photocatalytic Benzene Degradation

LI Zhao-Hui LIU Ping FU Xian-Zhi*
(*State Key Laboratory Breeding Base of Photocatalysis, Research Institute of Photocatalysis, Fuzhou University, Fuzhou 350002, P. R. China*)

Abstract: Benzene has severe health and environmental consequences because of its high toxicity and carcinogenicity. Although TiO_2-based photocatalytic oxidation (PCO) has been established as one of the most promising technologies for environmental remediation and has been successful in treating a wide variety of volatile organic compounds (VOCs), PCO has only limited success in the treatment of aromatic compounds like benzene because of the deactivation of TiO_2. The development of high performance photocatalysts for benzene degradation is indispensable for benzene treatment. Recently a series of wide bandgap *p*-block metal oxides/hydroxides with superior performance for the photocatalytic degradation of benzene have been developed in our institute. These wide bandgap *p*-block metal oxides/hydroxides are a series of promising photocatalysts for benzene degradation. In this article, the preparations of these *p*-block metal oxides/hydroxides, their photocatalytic activity and mechanism for benzene degradation as well as the structure-activity relationship are summarized.

Key Words: Photocatalysis; Benzene; Degradation; *p*-Block metal oxides/hydroxides

Benzene has severe health and environmental consequences due to its high toxicity and confirmed carcinogenicity[1–3]. A recent study has shown that a long-term exposure to a very low levels (volume fraction less than 1×10^{-6}) of benzene can reduce blood

Received: November 6, 2009; Revised: December 16, 2009; Published on Web: January 19, 2010.

*Corresponding author. Email: xzfu@fzu.edu.cn. Tel/Fax: +86-591-83738608.

The project was supported by the National Natural Science Foundation of China (20677009) and National Key Basic Research Program of China (973) (2007CB613306)
国家自然科学基金重点项目(20677009), 国家重点基础研究发展计划项目(973)(2007CB613306)资助.

付贤智. 1978–1991 年在北京大学化学系物理化学专业学习, 先后获得理学学士、理学硕士和理学博士学位. 1991–1993 年在北京大学从事博士后研究.

cell counts in human being. Workers exposed to benzene fumes, run into an increased risk of leukemia and bone-marrow toxicity[4]. Benzene is also ubiquitous as an air pollutant from cigarette smoke, gasoline vapors, paint, industrial exhaust gases, and automobile emissions. The benzene pollution has already become one of the main environmental problems facing humanity. Therefore, the development of an efficient, cost-effective and environmentally sustainable technology in treating benzene and its derivatives is indispensable.

Semiconductor photocatalysis for environmental remediation has received increasingly interest since it is environmentally friendly, capable of performing at room temperature and can treat organic pollutants at extremely low concentrations[5–13]. The photocatalytic reactions occur over the semiconductor photocatalysts are initiated by the photo-generated electrons and holes that are captured subsequently by the surface adsorbed species. The capture of photo-generated charge carriers induce the formation of very reactive radicals such as $O_2^{-\bullet}$, $O_2^{\bullet}$, $HO_2^{\bullet}$, $OH^{\bullet}$ and so on, leading to the final decomposition of organic pollutants[6].

Due to its high stability, non-toxicity, cheapness as well as its appropriate electronic band positions capable of oxidizing most organic pollutants, titanium dioxide (TiO_2) has become the most widely used semiconductor photocatalyst in heterogeneous photocatalysis. Although TiO_2-based photocatalytic oxidation (PCO) has been established to be one of the most promising technologies for the environment remediation and has been successful in treating a wide variety of volatile organic compounds (VOCs), PCO meets with limited success in the treatment of aromatic compounds like benzene due to the deactivation of TiO_2 resulted from the accumulation of the stable reaction intermediates on the surface[14–15]. Loading of noble metals like Pt, Pd, or Rh over TiO_2 has been used to enhance its performance for photocatalytic oxidation of benzene in gas phase. However, these noble-metal-loaded TiO_2 suffer from the problem of stability due to the oxidation of the noble metal nanoparticles on the surface of TiO_2[16–18]. Adding sufficient amount of H_2O in the reaction feed gas can improve the efficiency of TiO_2 photocatalyst toward the complete oxidization of benzene to a certain degree[19–20]. Our recent studies have also demonstrated that the introduction

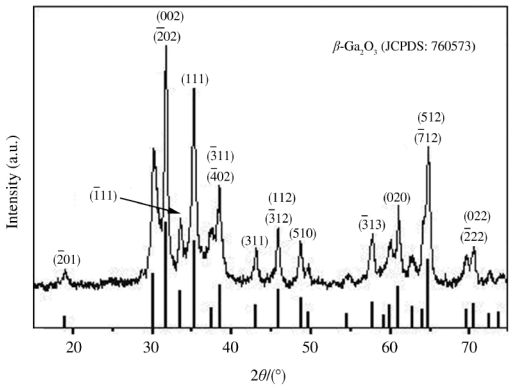

Fig.1 X-ray diffraction pattern of the as-synthesized Ga_2O_3 sample[24]

of magnetic field[21] or H_2[22–23] into the photochemical reaction system can greatly improve the efficiency of Pt/TiO_2 for the photodecomposition of benzene at room temperature. However, it is not easy to realize such a complicated hybrid system for photocatalytic air purification. Therefore the development of photocatalysts with high performance for benzene degradation is indispensable in view of the application of photocatalysis for ben–zene treatment, yet it remains a great challenge till now.

Recently, a series of wide band gap *p*-block metal oxides/hydroxides with superior performance for photocatalytic degradation of benzene have been developed in our institute[24–29]. These wide band gap *p*-block metal oxides/hydroxides are a series of promising photocatalysts for benzene degradation. The preparations of these *p*-block metal oxides/hydroxides, their photocatalytic activity and mechanism for benzene degradation as well as the structure-activity relationship are summarized in this review.

1 Preparations and photocatalytic activity for benzene degradation

1.1 Binary *p*-block metal oxides/hydroxides β-Ga_2O_3, $In(OH)_3$ and InOOH

Porous binary gallium oxide β-Ga_2O_3 can be prepared *via* the hydrolysis of gallium nitrate in ammonia solution followed by a heat treatment at 600 ℃[24]. The XRD pattern of the as-prepared

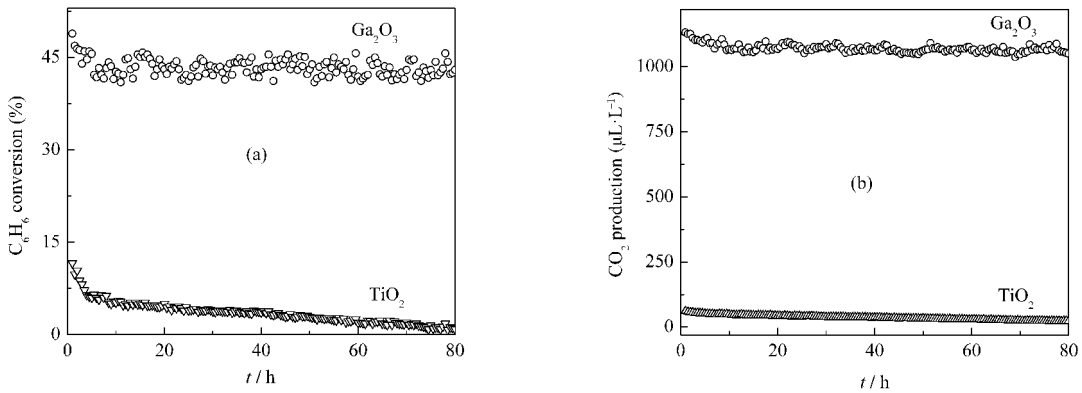

Fig.2 (a) Conversion of C_6H_6 and (b) the amount of produced CO_2 over the Ga_2O_3 as a function of reaction time, with TiO_2 (P25) as a reference[24]

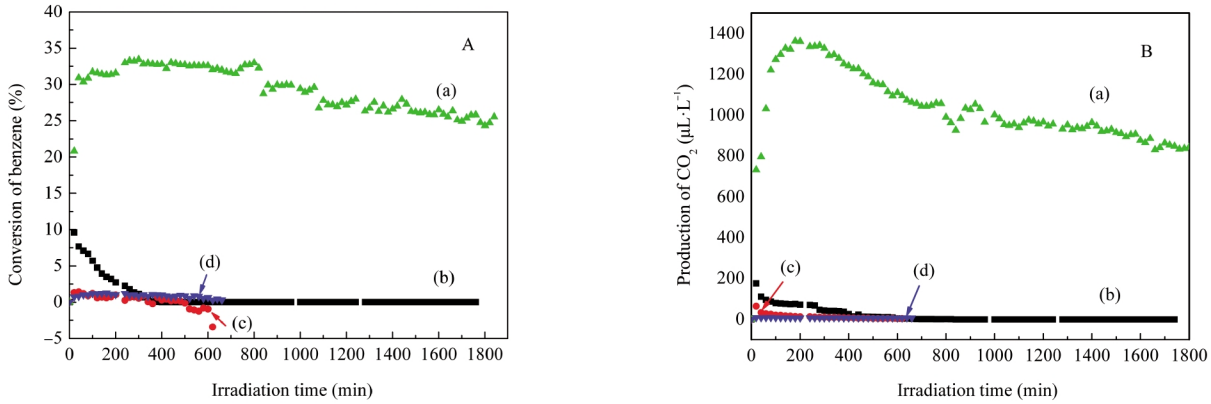

Fig.3 Photocatalytic oxidation conversion of henzene (A) and production of CO_2 (B) over the catalyst in dry O_2[25]

(a) $In(OH)_3$, (b) TiO_2; curve (c) was a control experiment with $In(OH)_3$ without irradiation, and (d) was a control experiment without $In(OH)_3$ under 254 nm irradiation; the initial benzene volume fraction: 1300×10^{-6}

β-Ga_2O_3 is shown in Fig.1. The as-prepared β-Ga_2O_3 exhibits stepwise adsorption and desorption (type IV isotherm) in the N_2-sorption isotherm, indicative of a porous solid. The BET specific surface area is 80 $m^2\cdot g^{-1}$ and the average pore size is 7.3 nm with a narrow distribution of pore size for the as-prepared β-Ga_2O_3. With a band gap of 4.7 eV, β-Ga_2O_3 can be excited with 254 nm UV irradiation. The as-prepared β-Ga_2O_3 is highly photoactive for mineralizing benzene and its derivatives like toluene and ethylbenzene to CO_2 under 254 nm UV irradiation. For an initial benzene volume fraction of 450×10^{-6}, β-Ga_2O_3 shows a high conversion rate of 42% and can maintain its reactivity during the prolonged operation of 80 h. In the meantime about 1070×10^{-6} of CO_2 can be produced over β-Ga_2O_3, indicating that 95% of benzene converted has been mineralized to CO_2 over β-Ga_2O_3 (Fig.2)[24].

Binary *p*-block metal hydroxide $In(OH)_3$ also shows high photocatalytic performance for benzene degradation under 254 nm UV irradiation. Porous $In(OH)_3$ can be prepared by hydrolysis of $In(NO_3)_3$ in an aqueous solution of ammonium followed by a thermal treatment at 120 ℃. The BET specific surface area for the as-prepared $In(OH)_3$ is 120 $m^2\cdot g^{-1}$. For an initial benzene concentration of 1300×10^{-6}, the conversion of benzene and the mineralization rate over $In(OH)_3$ can maintain at 25% and 40%, respectively, even after 30 h photocatalytic reaction (Fig.3)[25].

Oxyhydroxide InOOH can be prepared *via* a facile solvothermal process from $In(NO_3)_3$ in a water/ethylenediamine (1∶6) solution. The XRD pattern of the as-prepared InOOH is shown in Fig.4. The average particle size is about 20 nm and the BET specific surface area is about 55 $m^2\cdot g^{-1}$ for the as-prepared InOOH. With a band gap energy of 3.7 eV, InOOH can be excited by 300 nm UV irradiation. For an initial benzene concentration of 260×10^{-6}, the conversion of benzene over InOOH can reach 7.5%. In addition, the amount of the produced CO_2 is about 50×10^{-6}, corresponding to a benzene mineralization ratio of more than 50%. The photocatalytic activity can be maintained for more than 30 h, during which no noticeable deactivation is observed (Fig.5)[26].

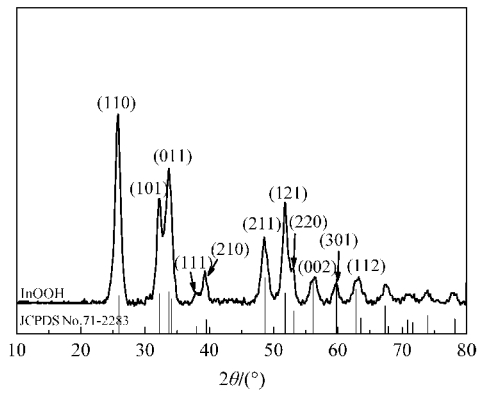

Fig.4 X-ray diffraction pattern of the as-prepared InOOH[26]

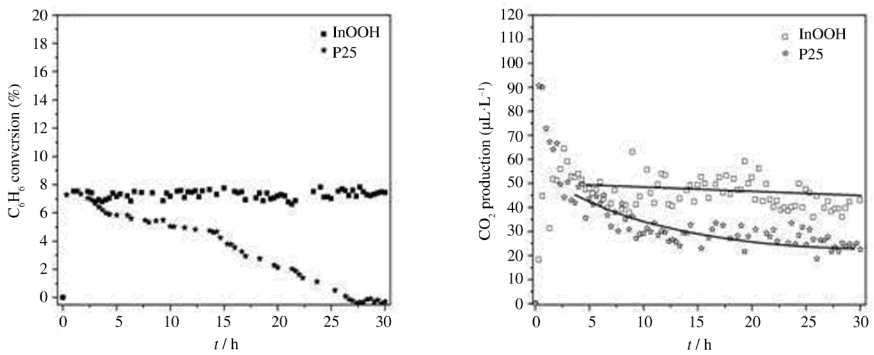

Fig.5 (A) Conversion of benzene and, (B) the amount of produced CO_2 over InOOH and P25 for decomposing benzene as a function of reaction time under UV illumination (λ=300 nm)[26]

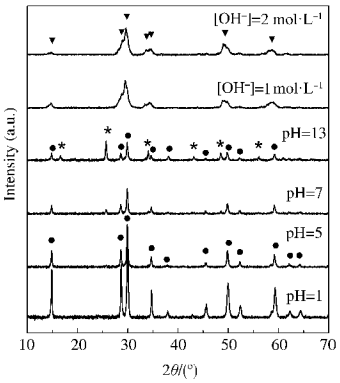

Fig.6 X-ray diffraction pattern of the samples prepared at 180 ℃ for 48 h with different pH values[27]

(●) $Sr_{1.36}Sb_2O_6$, (*) $SrSb_2O_6$, (▼) $Sr_2Sb_2O_7$

1.2 Ternary *p*-block metal semiconductors $Sr_2Sb_2O_7$, $ZnGa_2O_4$ and Zn_2GeO_4

Besides the binary *p*-block metal oxides/hydroxides, the photocatalytic activity for benzene degradation can also be found over ternary *p*-block metal oxides with more diversified composition and structure.

Nanocrystalline $Sr_2Sb_2O_7$ prepared *via* a facile hydrothermal method is found to show high activity for benzene degradation. Although $Sr_2Sb_2O_7$ prepared *via* a conventional solid state reaction method ($Sr_2Sb_2O_{7(SSR)}$) has been reported to be a photocatalyst for water splitting [30] and the degradation of organic dyes [31], it shows very low activity for benzene degradation due to its low specific surface area. To extend its application for photocatalytic degradation of benzene, we developed for the first time a facile method in the preparation of nanocrystalline $Sr_2Sb_2O_7$ directly from commercial Sb_2O_5. The XRD patterns of the obtained products under different pH values are shown in Fig.6. It is found that the reaction pH plays an important role in the final product and only under highly basic condition can nanocrystalline $Sr_2Sb_2O_7$ be obtained. The hydrothermal prepared nanocrystalline $Sr_2Sb_2O_7$ consists entirely of small particles with average size at around 6 nm and has a relatively large BET specific surface area of about 24.8 $m^2 \cdot g^{-1}$, much higher than $Sr_2Sb_2O_7$ prepared *via* the solid state reaction (1.4 $m^2 \cdot g^{-1}$). The N_2-sorption isotherm indicates that the as-prepared $Sr_2Sb_2O_7$ is a mesoporous solid with a narrow distribution of pore size at ca 4.0 nm. The as-prepared nanocrystalline $Sr_2Sb_2O_7$ show high photocatalytic performance for the degradation of benzene. For an initial benzene concentration of 220×10^{-6}, the conversion of benzene is about 24% and more than 160×10^{-6} of CO_2 is produced in the meantime, corresponding to a high mineralization ratio of about 50%. Both the conversion ratio and the mineralization ratio are higher than those over solid state prepared $Sr_2Sb_2O_7$ (4%, 30×10^{-6}). The high conversion and mineralization ratio can be maintained for more than 40 h, during which no obvious deactivation is observed (Fig.7)[27].

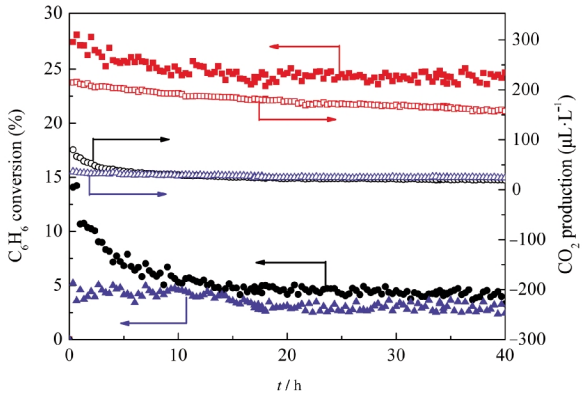

Fig.7 Conversion of C_6H_6 and the amount of produced CO_2 over the $Sr_2Sb_2O_7$ (180 ℃, 48 h, $[OH^-]=2$ mol·L^{-1}) as a function of reaction time, with TiO_2 (P25) and $Sr_2Sb_2O_{7(SSR)}$ as references[27]

(■) (●) (▲) the conversion of C_6H_6 over the $Sr_2Sb_2O_7$, TiO_2 and $Sr_2Sb_2O_{7(SSR)}$ respectively; (□) (○) (Δ) the amount of produced CO_2 over the $Sr_2Sb_2O_7$, TiO_2 and $Sr_2Sb_2O_{7(SSR)}$ respectively. $Sr_2Sb_2O_{7(SSR)}$ refer to the sample prepared *via* a solid state reaction

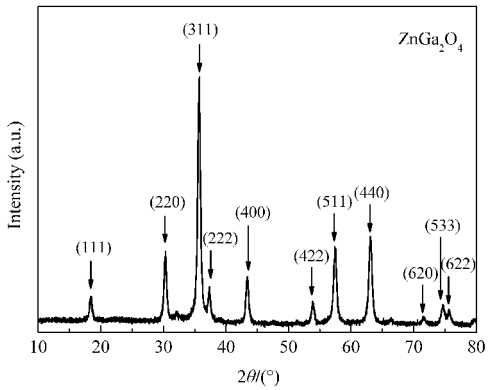

Fig.8 X-ray diffraction pattern of the nanocrystalline $ZnGa_2O_4$[28]

Nanocrystalline $ZnGa_2O_4$ with a specific surface area of about 36.7 $m^2 \cdot g^{-1}$ can be prepared *via* a co-precipitation method from $Zn(NO_3)_2$ and $Ga(NO_3)_3$ followed by a heat treatment at 600 ℃. The XRD pattern of the as-prepared $ZnGa_2O_4$ is shown Fig.8. For an initial benzene concentration of 220×10^{-6}, the conversion of benzene over the thus-prepared $ZnGa_2O_4$ is about 12.0% and

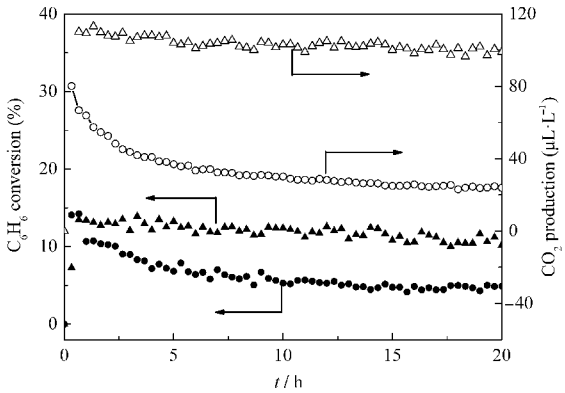

Fig.9 Conversion of C_6H_6 and the amount of produced CO_2 over the nanocrystalline $ZnGa_2O_4$ as a function of reaction time, with TiO_2 (P25) as references[28]

(▲) (●) the conversion of C_6H_6 over the $ZnGa_2O_4$ and TiO_2 respectively, (Δ) (○) the amount of produced CO_2 over the $ZnGa_2O_4$ and TiO_2 respectively.

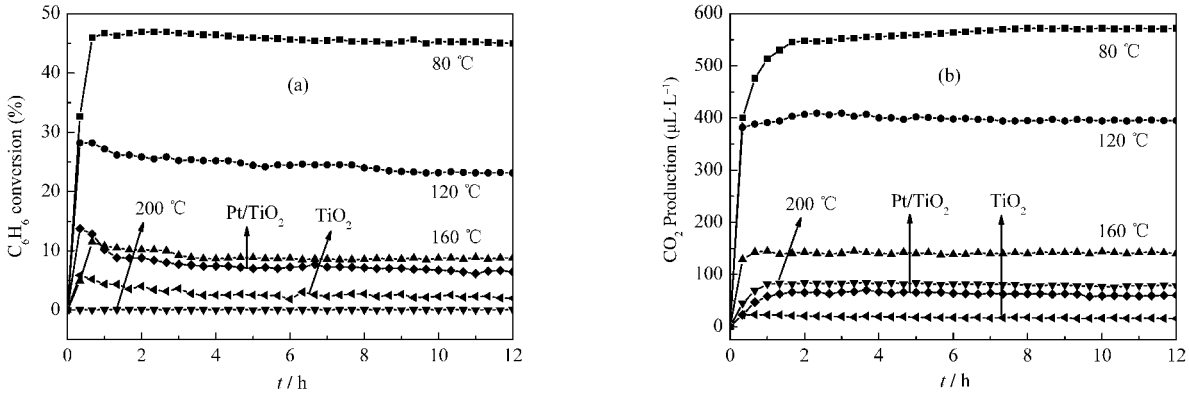

Fig.10 Photocatalytic conversion of benzene (a) and the amount of produced CO_2 (b) over $ZnGa_2O_4$ hydrothermal prepared under 80, 120, 160, 200 ℃, TiO_2 and Pt/TiO_2[32]

more than 100×10^{-6} of CO_2 can be produced, corresponding to a mineralization ratio of about 63% (Fig.9)[23]. With an aim at enhancing its activity, $ZnGa_2O_4$ with an extremely high specific surface area of 201 $m^2\cdot g^{-1}$ has been prepared from $Zn(NO_3)_2$ and $Ga(NO_3)_3$ *via* a hydrothermal treatment at 80 ℃. The increase of the specific surface area leads to a significant enhancement of the photocatalytic activity for benzene degradation. The conversion ratio of benzene can be increased to as high as 41% and the produced CO_2 can reach 500×10^{-6} for an initial benzene concentration of 300×10^{-6}, which is much higher than Pt/TiO_2 (Fig. 10)[32].

Another ternary *p*-block metal oxides with high photocatalytic performance for benzene degradation is Zn_2GeO_4. Nanorods of Zn_2GeO_4 can be prepared from GeO_2 and $Zn(Ac)_2$ under the assistance of surfactant cetyltrimethylammonium bromide (CTAB) *via* a facile hydrothermal method and the XRD pattern is shown in Fig.11. The SEM images reveal that the as-prepared sample contains a large quantity of nanorods 20–50 nm in width and 150–600 nm in length (Fig.12). Under 254 nm UV irradiations, for an initial benzene concentration of 300×10^{-6}, the benzene conversion and CO_2 concentration over the as-prepared Zn_2GeO_4 nanorods can be maintained steady at ca 21% and ca 280×10^{-6}, respectively, which corresponding to a high mineralization ratio of ca 75% (Fig.13)[29].

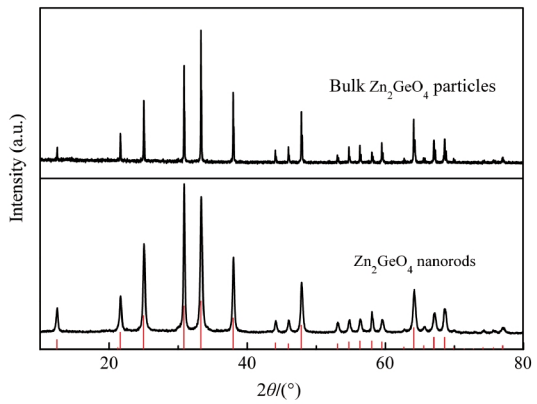

Fig.11 X-ray diffraction pattern of Zn_2GeO_4 nanorods and bulk Zn_2GeO_4 particles[29]

2 Structure-activity relationship

The band gap, crystallinity, and the specific surface area are important factors that can influence the photocatalytic activity of the semiconductor photocatalysts. However, the activity of some *p*-block metal oxide photocatalysts can not be simply explained in terms of the above factors. A study on three crystalline phase of Ga_2O_3 reveals that the intrinsic crystallographic structure, especially the geometric structure of the M—O polyhedron (M=*p*-block metal) can influence the photocatalytic activity of these wide band gap semiconductors as well[33]. The crystal structure of α-Ga_2O_3 and β-Ga_2O_3 (Fig.14) and the calculations using the crystallographic data regarding the atom positions reveal that α-Ga_2O_3 is constituted only by distorted octahedron GaO_6 with a dipole moment of 14.0×10^{-30} C·m, while β-Ga_2O_3 contains both distorted GaO_6 octahedron (7.3×10^{-30} C·m) and GaO_4 tetrahedron (2.3×10^{-30} C·m). It is believed that the dipole moment induced by the distorted polyhedron can create a local electric field inside the distorted polyhedron, which can promote the separation of the photo-generated electron-hole pairs[34]. Although both α-Ga_2O_3 and β-Ga_2O_3 contain distorted polyhedron in their structure, α-Ga_2O_3 contains only distorted octahedron, while β-Ga_2O_3 has both heavily distorted octahedron and tetrahedron in

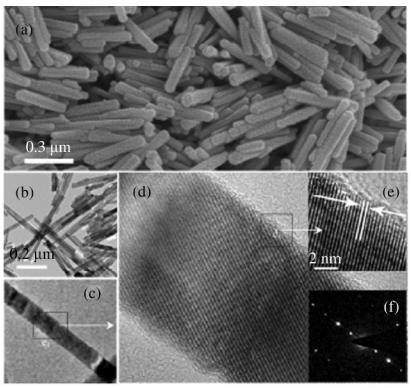

Fig.12 Structural characterization and general morphology of Zn_2GeO_4 nanorods[29]

(a) SEM image, (b) TEM image, (c) TEM image of a Zn_2GeO_4 nanorod, (d) HRTEM image of area e1 in (c), (e) enlarged image of area f1 in (d), (f) SAED pattern recorded along the zone axis [110] of the Zn_2GeO_4 nanorods

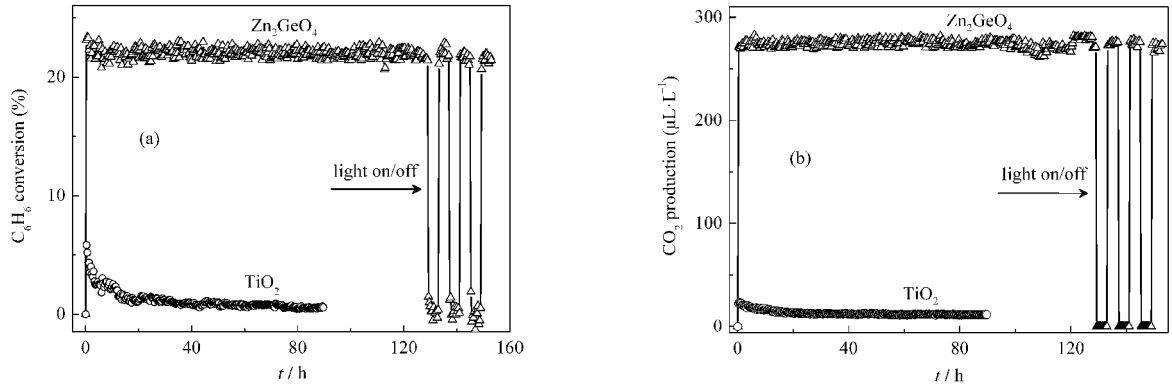

Fig.13 (a) Photocatalytic conversion of benzene and (b) amount of produced CO_2 in the stream over the Zn_2GeO_4 nanorods against the reaction time, with TiO_2 (Degussa P25) as a reference catalyst[29]

Table 1 Hydrocarbon removal rate and CO_2 production rate over different photocatalysts[33]

Sample	S_{BET}/($m^2 \cdot g^{-1}$)	Hydrocarbon removal rate ($\mu mol \cdot h^{-1} \cdot m^{-2}$)			CO_2 production rate ($\mu mol \cdot h^{-1} \cdot m^{-2}$)		
		C_6H_6	C_7H_8	C_8H_{10}	C_6H_6	C_7H_8	C_8H_{10}
α-Ga_2O_3	58	0.32	0.46	0.31	1.7	1.3	1.2
β-Ga_2O_3	80	0.42	0.52	0.36	2.4	1.8	1.6
γ-Ga_2O_3	135	0.21	0.26	0.20	0.95	0.85	0.73
TiO_2-P25	50	0.08	0.15	0.18	0.17	0.13	0.15

The values are obtained at 12 h.

Table 2 Lifetimes (τ) and relative amplitudes of time-resolved photoluminescence of the gallium oxide catalysts at 77 K[33]

	τ_1/μs	τ_2/μs	τ_3/μs
α-Ga_2O_3	3.2 (28%)	15 (43%)	109 (29%)
β-Ga_2O_3	5.8 (26%)	24 (36%)	142 (38%)
γ-Ga_2O_3	2.9 (38%)	13 (46%)	89 (17%)

Excited at 254 nm and monitored at 490 nm, the data in brackets are the relative amplitudes.

its structure. The coexistence of two different kinds of electric fields might have synergic effects in promoting the separation of photoexcited electron-hole pairs. Therefore, α-Ga_2O_3 shows a lower photocatalytic activity than β-Ga_2O_3 (Table 1). This promoting effect is confirmed by the time-resolved photoluminescence (PL) measurements. The PL measurements reveal that the lifetime of the photogenerated electron-hole pairs on β-Ga_2O_3 is longer than that on α-Ga_2O_3 (Fig.15 and Table 2). The existence of the relationship between the geometric structure and the photocatalytic activity among these semiconductor photocatalysts provides some guideline in our development of new wide band gap *p*-block metal semiconductor photocatalysts.

3 Mechanism for benzene degradation

All the above mentioned wide band gap *p*-block metal oxides/hydroxides show high stability for benzene degradation, while TiO_2 deactivate very quickly. Their obvious different behavior implies that these *p*-block metal oxides/hydroxides and TiO_2 may have different routes in the photocatalytic degradation of benzene.

Generally, it is believed that the degradation of benzene over TiO_2 under dry air proceeds preferentially *via* a direct-hole-oxidation route. Such a direct-hole-oxidation process would produce benzene cationic radical, which react further with an incoming benzene molecule, leading to the polymerization of benzene on the catalyst surface and the deactivation of TiO_2 during the degradation of benzene[35]. The deposition of the stable intermediates can be confirmed by the color change of TiO_2 from the original white to dark brown after the photocatalytic reaction. In addition to this, the FT-IR spectrum of used TiO_2 indicates the formation of the stable intermediates by showing three new peaks at 1483, 1686 and 1711 cm^{-1} (Fig.16). On the contrary, no color change has been observed after photocatalytic benzene degradation for the *p*-block metal oxides/hydroxides, like InOOH. Besides this, no new peaks appear on the FT-IR spectrum over these *p*-block metal oxides/hydroxides, indicating that no stable intermediates have been deposited on the surface

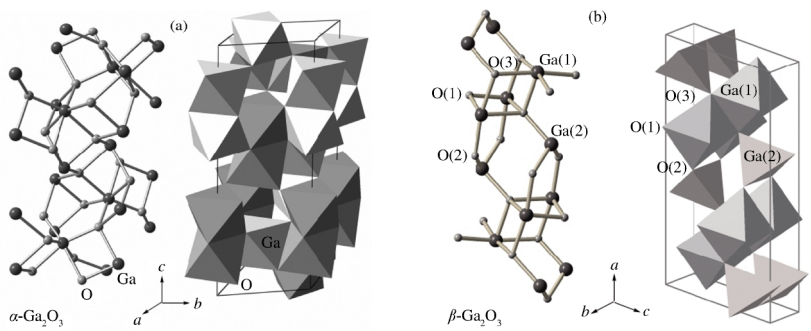

Fig.14 Three-dimensional crystal structures of α-Ga_2O_3 and β-Ga_2O_3 with a unit cell[33]

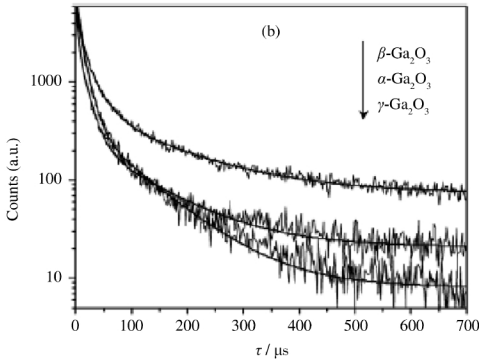

Fig.15 Photoluminescence decay curves of the gallium oxide catalysts[33]

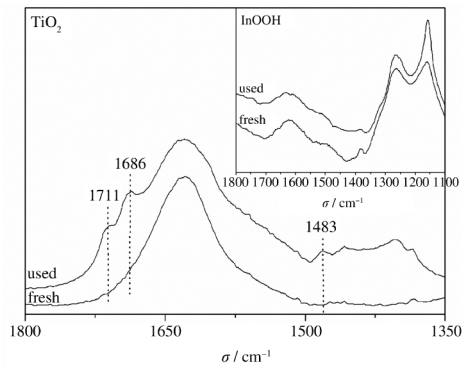

Fig.16 FT-IR spectra of used and fresh P25 and InOOH (inset)[26]

of these photocatalysts (Fig.16). All these phenomena imply that the degradation of benzene over these *p*-block metal oxides/hydroxides may proceed preferentially *via* the HO· radical route. Photocatalysts proceed *via* the HO· radical degradation route may have long term stability since the HO· radical route could significantly suppress the polymerization of benzene on the catalyst surface.

The generation of HO· radicals over these *p*-block metal oxides/hydroxides is credible since they all have proper band structure. The calculations of their band position based on the following equation: $E_{CB}=X-E_c-0.5E_g$ is −0.4 V (*vs* NHE)[36] reveal that the edge of their conduction band are all negative than that of $E(O_2/O_2^{-\bullet})$ (−0.33 V *vs* NHE), while the edge of their valence band (E_{VB}) are positive than that of $E(HO\cdot/OH^-)$ (2.38 V *vs* NHE)[37]. These suggest that the photogenerated electrons on these *p*-block metal oxides/hydroxides can reduce O_2 to give $O_2^{-\bullet}$, while the photogenerated holes can oxidize OH^- to give HO· when illuminated. The ESR spin-trap with DMPO technique confirmed the production of both $O_2^{-\bullet}$ and HO· over all these *p*-block metal oxides/hydroxides. In addition to this, it is observed that the intensities of the signal corresponding to the DMPO-HOo radical produced over the *p*-block metal oxides/hydroxides (for example, InOOH) are much stronger than those over P25 (Fig.17). This indicates that under similar condition, more HO· radicals can be produced over irradiated *p*-block metal oxides/hydroxides than over P25[26]. This again confirms the above assumption that the degradation of benzene over *p*-block metal oxides/hydroxides may proceeds preferentially *via* the HO· radical route, while that over P25 may proceed *via* the direct-hole oxidation route.

The degradation preferentially *via* the HO· radical route over these *p*-block metal oxides/hydroxides can be attributed to their peculiar structure. The intrinsic wide band gap of these *p*-block metal oxides/hydroxides endow the photogenerated holes with strong oxidation ability and make them thermodynamically more favorable to react with chemi-adsorbed H_2O or the surface hydroxyl group to produce HO· radicals. On the other hand, the highly dispersive conduction band due to the hybridizations of the orbitals usually observed over these *p*-block metal oxides/hydroxides can promote the mobility of the photoexcited electrons, leading to enhanced charge separation. All these characteristics are favorable for the generation of the HO· radicals over these *p*-block metal oxides/hydroxides when illuminated. Therefore the degradation of benzene over these *p*-block metal oxides/hydroxides can proceed preferentially *via* HO· radical route and hence a high stability is observed.

The possible benzene degradation mechanism over these wide band gap *p*-block metal oxides/hydroxides is illustrated in Scheme 1. When illuminated, these *p*-block metal oxides/hydroxides can be efficiently excited to create electron-hole pairs.

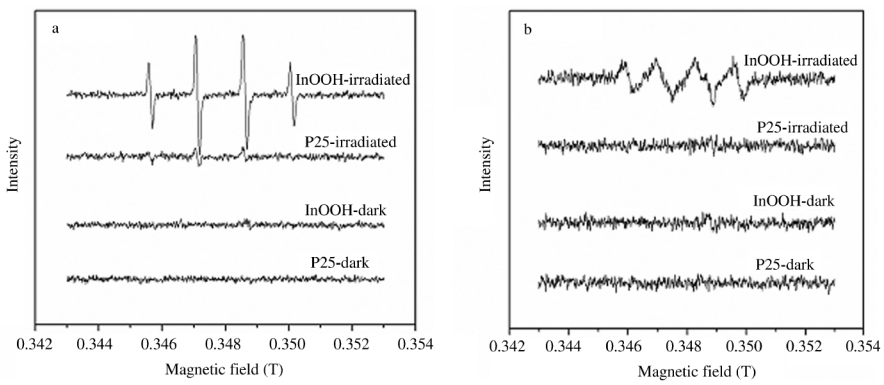

Fig.17 DMPO spin-trapping ESR spectra (a) in aqueous dispersion for DMPO-·OH and (b) in methanol dispersion for DMPO-$O_2^{-\bullet}$[26]

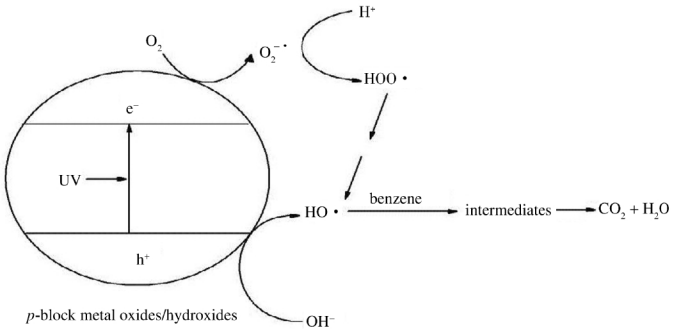

Scheme 1 Possible mechanism of the photocatalytic degradation of benzene over wide band gap *p*-block metal oxides/hydroxides

The photogenerated electrons and holes are long-lived enough to react with adsorbed H_2O or surface hydroxyl group to produce HO· radicals. Since the water content in the feed gas is maintained at such a low level ($<5\times10^{-6}$), H_2O involved in the generation of the HO· radicals must come from the photocatalytic reaction itself. The photocatalytic degradation of benzene over these *p*-block metal oxides/hydroxides can proceed preferentially *via* the HO· radical. In this way, no polymerized intermediates can be deposited and these *p*-block metal oxides/hydroxides can maintain a clean surface and a higher stability in the photodegradation of benzene.

4 Conclusions and outlook

Wide band gap *p*-block metal oxides/hydroxides can be a promising new generation of photocatalysts for benzene degradation. Their superior photocatalytic performance for benzene degradation may be attributed to their peculiar structures and their mechanism different from TiO_2 in the degradation of benzene. A limitation for the application of these wide band gap *p*-block metal oxides/hydroxides in the practical environmental remediation is their wide band gap since they can only adsorb the UV energy, which account for only ca 4% of the solar energy. Since the ultimate goal of photocatalysis is to use the solar light, the application of the photocatalysis of these wide band gap semiconductors in the visible light region is important. The extension of the adsorption of these wide band gap semiconductors to the visible light region is still going on in our lab.

References

1 Hudak, A.; Ungvary, G. *Toxicology*, **1978, 11**: 55

2 Caprino, L.; Togna, G. I. *Environ. Health Perspect.*, **1998, 106**: 115

3 Bird, M. G.; Greim, H.; Snyder, R.; Rice, J. M. *Chem. -Biol. Interact.*, **2005, 153**: 1

4 Lan, Q.; Zhang, L.; Li, G.; Vermeulen, R. V.; Weinberg, R. S.; Dosemeci, M.; Rappaport, S. M.; Shen, M.; Alter, B. P.; Wu, Y.; Kopp, W.; Waidyanatha, S.; Rabkin, C.; Guo, W.; Chanock, S.; Hayes, R. B.; Linet, M.; Kim, S.; Yin, S.; Rothman, N.; Smith, M. T. *Science*, **2004, 306**: 1774

5 Mills, A.; Davies, R. H.; Worsley, D. *Chem. Soc. Rev.*, **1993, 22**: 417

6 Hoffman, M. R.; Martin, S. T.; Choi, W.; Bahnemann, D. W. *Chem. Rev.*, **1995, 95**: 69

7 Fujishima, A.; Rao, T. N.; Tryk, D. A. *J. Photochem. Photobiol. C*, **2000, 1**: 1

8 Linsebigler, L.; Lu, G.; Yates Jr., J. T. *Chem. Rev.*, **1995, 95**: 735

9 Fujishima, A.; Hashimoto, K.; Watanabe, T. Photocatalysis fundamentals and applications. 1st ed. Tokyo: BKC, 1999

10 Kaneko, M.; Okura, I. Photocatalysis, science and technology, Berlin: Springer, 2002

11 Serpone, N.; Pelizzetti, E. Photocatalysis: fundamentals and applications. New York: Wiley, 1989

12 Ollis, D. F.; Al-Ekabi, H. Photocatalytic purification and treatment of water and air. Amsterdam: Elsevier, 1993

13 Fox, M. A.; Dulay, M. T. *Chem. Rev.*, **1993, 93**: 341

14 Mendez-Roman, R.; Cardona-Martinez, N. *Catal. Today*, **1998, 40**: 353

15 Martra, G.; Coluccia, S.; Marchese, L.; Augugliaro, V.; Loddo, V.; Palmisano, L.; Schiavello, M. *Catal. Today*, **1999, 53**: 695

16 Fu, X. Z.; Zeltner, W. A.; Anderson, M. C. *Appl. Catal. B: Environ.*, **1995, 6**: 209

17 Einaga, H.; Futamura, S.; Ibusuki, T. *Environ. Sci. Technol.*, **2001, 35**: 1880

18 Einaga, H.; Futamura, S.; Ibusuki, T. *Environ. Sci. Technol.*, **2004, 38**: 285

19 Sitkiewitz, S.; Heller, A. *New J. Chem.*, **1996, 20**: 233

20 Einaga, H.; Futamura, S.; Ibusuki, T. *Phys. Chem. Chem. Phys.*, **1999, 1**: 4903

21 Zhang, W.; Wang, X. X.; Fu, X. Z. *Chem. Commun.*, **2003**: 2196

22 Chen, Y. L.; Li, D. Z.; Wang, X. C.; Wang, X. X.; Fu, X. Z. *Chem. Commun.*, **2004**: 2304

23 Chen, Y. L.; Li, D. Z.; Wang, X. C.; Wang, X. X.; Fu, X. Z. *New J. Chem.*, **2005, 29**: 1514

24 Hou, Y. D.; Wang, X. C.; Wu, L.; Ding, Z. X.; Fu, X. Z. *Environ. Sci. Technol.*, **2006, 40**: 5799

25 Yan, T. J.; Long, J. L.; Chen, Y. S.; Wang, X. X.; Li, D. Z.; Fu, X. Z. *C. R. Chim.*, **2008, 11**: 101

26 Li, Z. H.; Xie, Z. P.; Zhang, Y. F.; Wu, L.; Wang, X. X.; Fu, X. Z. *J. Phys. Chem. C*, **2007, 111**: 18348

27 Xue, H.; Li, Z. H.; Wu, L.; Ding, Z. X; Wang, X. X.; Fu, X. Z. *J. Phys. Chem. C*, **2008, 112**: 5850

28 Chen, X.; Xue, H.; Li, Z. H.; Wu, L.; Wang, X. X.; Fu, X. Z. *J. Phys. Chem. C*, **2008, 112**: 20393

29 Huang, J. H.; Wang, X. C.; Hou, Y. D.; Chen, X. F.; Wu, L.; Fu, X. Z. *Environ. Sci. Technol*., **2008, 42**: 7387

30 Sato, J.; Saito, N.; Nishiyama, H.; Inoue, Y. *J. Photochem. Photobio. A*: *Chem*., **2002, 148**: 85

31 Lin, X. P.; Huang, F. Q.; Wang, W. D.; Wang Y. M.; Xia, Y. J.; Shi, J. L. *Appl. Catal. A*: *Gen*., **2006, 313**: 218

32 Zhang, X.; Huang, J.; Ding, K.; Hou, Y.; Wang, X.; Fu, X. *Environ. Sci. Technol*., **2009, 43**: 5947

33 Hou, Y.; Wu, L.; Wang, X.; Ding, Z.; Li, Z.; Fu, X. *J. Catal*., **2007, 250**(1): 12

34 Sato, J.; Kobayashi, H.; Inoue, Y. *J. Phys. Chem. B*, **2003, 107**: 7970

35 d′Hennezel, O.; Pichat, P.; Ollis, D. F. *J. Photochem. Photobiol. A*, **1998, 118**: 197

36 Butler, M. A.; Ginley, D. S. *J. Electrochem. Soc*., **1978, 125**: 228

37 Bard, A. J.; Parsons, R.; Jordan, J. Standard potentials in aqueous solution. New York: Marcel Dekker, 1985